Radiocarbon and Luminescence Dating of Lacustrine Sediments in Zhari Namco, Southern Tibetan Plateau

Lu Cong[1,2,3], Yixuan Wang[1]*, Xiying Zhang[2], Tianyuan Chen[2], Donglin Gao[2] and Fuyuan An[4]

[1] Key Laboratory of Comprehensive and Highly Efficient Utilization of Salt Lake Resources, Qinghai Institute of Salt Lakes, Chinese Academy of Sciences, Xining, China, [2] Key Laboratory of Salt Lake Geology and Environment of Qinghai Province, Xining, China, [3] University of Chinese Academy of Sciences, Beijing, China, [4] Key Laboratory of Physical Geography and Environmental Processes of Qinghai Province, School of Geographical Science, Qinghai Normal University, Xining, China

There are more than 1,000 lakes within the Tibetan Plateau (TP), all of which are sensitive to changes in regional climate and local hydrology. Lacustrine sediments within these lakes preserve a good record of these changes. However, determining their precise ages is difficult due to the complex nature of lake reservoir effects (LRE), which limit our understanding of paleoenvironmental changes. Focusing on an exposed 600 cm thick lacustrine sediment profile located in western Zhari Namco, we used a combination of both radiocarbon and optically stimulated luminescence (OSL) dating methods in order to evaluate the carbon reservoirs of bulk organic matter (BOM) and aquatic plant remnants (APR), and to explore the age differences between ^{14}C and OSL and their respective reliability. We demonstrated that (i) OSL ages were changed in stratigraphic order, and the OSL age just below the beach gravel layer was consistent with previously reported paleoshoreline ages; (ii) ^{14}C ages were divergent between BOM and grass leaves; (iii) ^{14}C ages of BOM were older than ^{14}C ages of APR; and (iv) all ^{14}C ages were older than OSL ages. This could be attributed to changing LRE in the past, causing the ^{14}C ages to appear unstable during the deposition period. Although the ^{14}C ages of terrestrial plant remnants (TPR) were not affected by LRE, an analyzed twig nonetheless returned a ^{14}C age older than its respective layer's OSL age, suggesting it may have been preserved on land prior to transportation into the lake. Our study suggests that OSL ages are more reliable than ^{14}C ages with respect to Zhari Namco lacustrine sediments. We recommend caution when interpreting paleoenvironmental changes based on lacustrine sediment ^{14}C ages alone.

Keywords: lake reservoir effect, lacustrine sediments, optically stimulated luminescence, radiocarbon dating, Tibetan Plateau

INTRODUCTION

The Tibetan Plateau (TP) is the largest and highest plateau on Earth, often regarded as the "Third Pole" due to both its high elevations and expansive *c.* 2.5 million km^2 coverage (Yao et al., 2012; Liu et al., 2019). Of the more than 1,400 lakes (larger than 1 km^2) distributed across the TP, *c.* 60% are within the endorheic TP (Zhang et al., 2020), and their lacustrine sediments preserve a wealth of

information that helps researchers track past environmental and hydrological changes within the region (Hou et al., 2010; Long et al., 2014; Liu et al., 2018; Chongyi et al., 2018).

Radiocarbon (^{14}C) dating is the most commonly used method for dating lacustrine sediments within the TP (Shen et al., 2005; Hou et al., 2010; Chen H. et al., 2019; Wang H. et al., 2019), with most age frameworks for borehole lacustrine sediments constructed using ^{14}C ages (Hou et al., 2012). Terrestrial plant remnants (TPR), aquatic plant remnants (APR), and bulk organic matter (BOM) are typical materials for ^{14}C dating of lacustrine sediments within the TP (Zhang et al., 2007). Although ^{14}C dating is a mature dating technology with high precision, the harsh environmental conditions in the region limit overall biomass. This makes it difficult to find TPR in lacustrine sediments (Mischke et al., 2013). However, ^{14}C ages taken from the BOM and APR of lacustrine sediments ^{14}C ages are often influenced by the disequilibrium with atmospheric radiocarbon, thus causing the corresponding BOM and APR ^{14}C ages to appear older than the ^{14}C ages of contemporaneous TPR. This phenomenon is called the lake reservoir effect (LRE), which is commonly encountered during radiocarbon dating of lacustrine sediments within the TP. The accurate estimation of LRE is a crucial prerequisite for establishing reliable ^{14}C age-depth relationships (Stuiver and Braziunas, 1993; Ascough et al., 2011). Hou et al. (2012) and Mischke et al. (2013) summarized several approaches for evaluating LRE within the TP. These methods include: ^{14}C-based estimation of reservoir ages (RAs) using modern lacustrine sediments (Mischke et al., 2010), linear extrapolation of the ^{14}C age-depth model to the sediment-water interface depth (Fontes et al., 1996; Shen et al., 2005), geochemical models for ^{14}C reservoir correction (Wang et al., 2007; Yu et al., 2007), stratigraphic alignment (Liu et al., 2008), independent age determinations such as ^{210}Pb and ^{137}Cs dating (Zhu et al., 2008), optically stimulated luminescence (OSL) dating (Long et al., 2014; Wang Y. X. et al., 2019), U-series dating (Zhu et al., 2004), magnetic susceptibility comparison (Li et al., 2021), and varve counting (Zhou et al., 2011). In the above methods, OSL is unaffected by variations in LRE and lake hydrochemistry, and it is convenient for extracting dating materials (e.g., quartz and feldspar grains). Because of these advantages, OSL dating is frequently used for Quaternary sediments dating.

The OSL age of sediment directly reflects its time of burial, i.e., when it was last exposed to sunlight (Aitken, 1998). Recent studies have successfully applied the OSL dating method to TP loess (Liu et al., 2012, 2017; Wang et al., 2018; Kang et al., 2020; Li et al., 2020), dunes (Chen T. Y. et al., 2019), sand wedges (Liu et al., 2010; Liu and Lai, 2013), river sediments (An et al., 2018) and lacustrine sediments (Liu et al., 2011, 2015) in order to reveal their respective accumulation histories. Moreover, many recent studies have used a combination of ^{14}C and OSL dating to discuss the reliability of ages from lacustrine sediment cores. Zhang et al. (2007) used OSL and ^{14}C dating in organic-rich lacustrine sediments cored from Lake Gucheng (Jiangsu, China), and found the ^{14}C ages of BOM were *c.* 2,000 years (a) older than the OSL ages. Shen et al. (2008) applied OSL dating using fine silt quartz, together with ^{14}C dating of terrestrial plant macrofossils, which should not have been affected by the LRE,

to establish a chronology for a lacustrine sediment core from Crummock Water (in the northwestern part of the English Lake District). Long et al. (2011) used OSL and ^{14}C dating of lacustrine sediments from Qingtu Lake (northern China); the apparent agreement between OSL and ^{14}C dating suggested that the RAs of ^{14}C samples in Qingtu Lake were much lower than in other lakes of northern China (e.g., Bangong Lake: 6,670 a, Fontes et al., 1996, Qinghai Lake: 1,039 a, Shen et al., 2005, Ahung Lake: 600–700 a, Morrill et al., 2006, Bositeng Lake: 1,140 a, Chen et al., 2006). However, only few studies of lacustrine sediments from the TP have used multi-dating approaches to establish age-depth models (Hu et al., 2017). Hu et al. (2017) used a combination of ^{210}Pb, ^{14}C, and OSL dating in Linggo Co (central TP) and found that the ^{210}Pb and OSL ages were roughly concordant, and all ^{14}C ages were much older than the ^{210}Pb and OSL ages at the same depths.

Therefore, a comparison between OSL and ^{14}C ages may help assess the reliability of the established chronology. In this study, ^{14}C ages sampled from different materials were compared with independently obtained OSL ages from Zhari Namco with the aim of determining their respective accuracy and reliability and to gain a better understanding of the intrinsic variability of the LRE.

STUDY AREA AND RESEARCH MATERIALS

Zhari Namco (30°44′–31°05′N, 85°20′–85°54′E) is a brackish lake located in the Cuoqin Basin, situated in the southern TP and possessing a cold and arid climate (**Figure 1**). The lake is formed by an east-west extending structural fault and is irregular in shape with narrow northern and southern banks, whereas its eastern and western banks are relatively wide. According to GPS measurements in the field, Zhari Namco sits at an elevation of 4,613 m above sea level (a.s.l.). With an overall length of 54.3 km from east to west, a length of 26.2 km from north to south, a present surface area of 996.9 km^2, and a catchment area of *c.* 15,433.2 km^2, it is the third-largest lake in Tibet after Siling Co and Namco. It is supplied mainly by precipitation and meltwater from snow and ice, with the Cuoqin Zangbo River—which drains into the lake from the south—representing the major water input. This river originates at the Gangdisê Mountains (*c.* 6,000 m a.s.l.) and has a total length of 253 km and a catchment area of about *c.* 9,930 km^2 (Wang and Dou, 1998).

An exposed section, named CQ (31°0′56.086″N, 85°8′51.238″E, elevation 4,664 m a.s.l.), was discovered in Cuoqin County, which is located on the west side of the lake. Section CQ (**Figure 2**) is composed of subsection CQ1 (**Figure 2A**) and CQ2 (**Figure 2B**). CQ1 is located at the top and is 400 cm thick. CQ2 is 200 cm thick and connects with the bottom of CQ1. The surface section of CQ is comprised mainly of modern soil and some gravels (0–5 cm). Moving up the section, the sediments change from fine to coarse, with the color undergoing an attendant change from dark to light. CQ can roughly be divided into five stratigraphic units: In the bottommost part (600–230 cm depth), the sediments are unstratified silty clay and fine sands with dark black coloration and exuding a strong smell of organic decay,
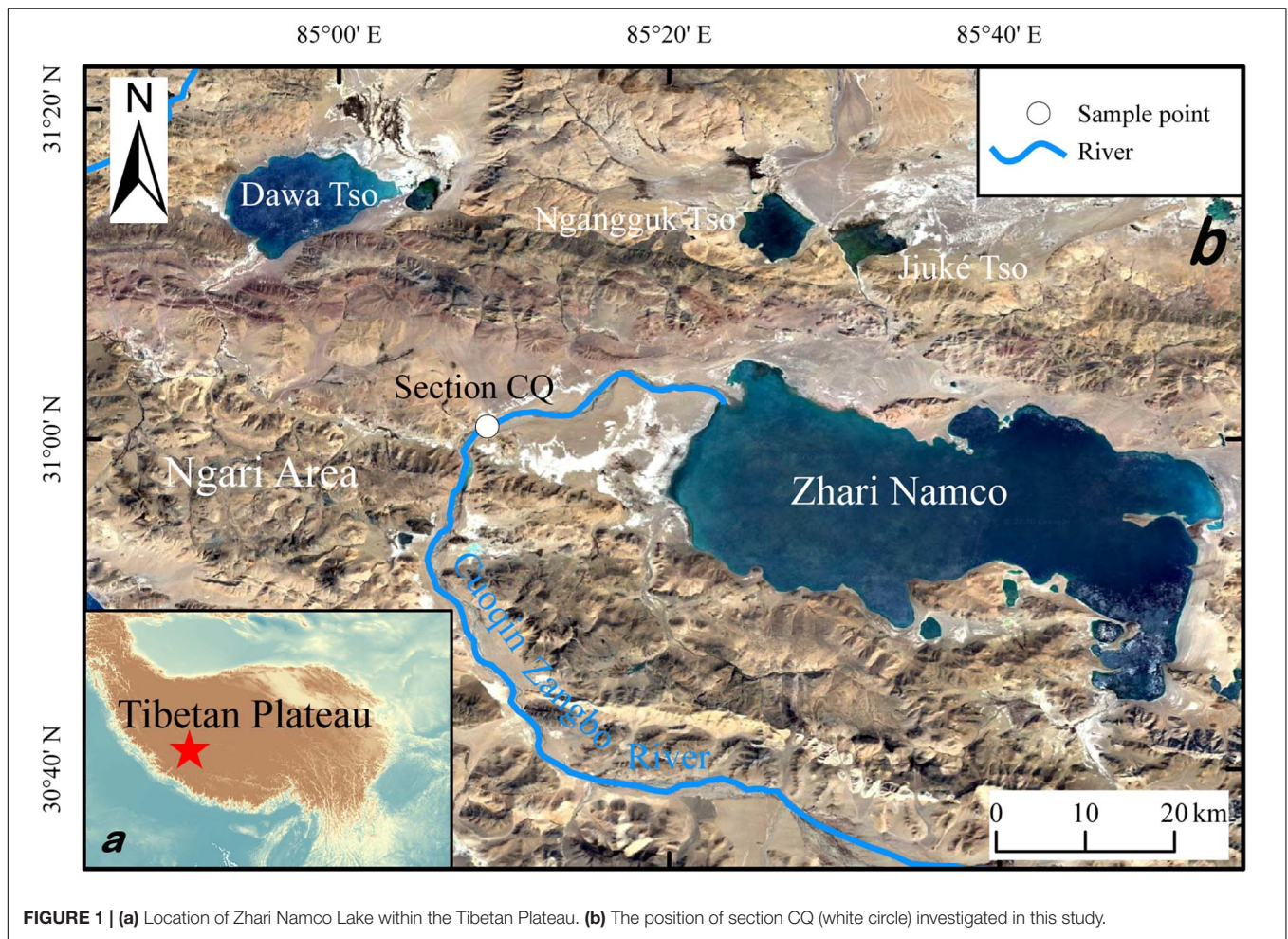
FIGURE 1 | (a) Location of Zhari Namco Lake within the Tibetan Plateau. **(b)** The position of section CQ (white circle) investigated in this study.

indicating continuous sedimentation within a deep and stable lake environment (**Figure 2a**). In the second part (230–150 cm depth), the sediments change from blackish to grayish medium-fine sands (**Figure 2b**). The third part (150–130 cm depth) is comprised of a layer of well-sorted, yellowish to grayish, medium-fine sands, indicating they were deposited at or near the lake shoreline (**Figure 2c**). The sediments of the fourth part (130–70 cm depth) consist of coarse sands and pebbles, which are round or dish-shaped with a long axis of 0.5 cm to 3 cm, indicative of a high-energy shoreline deposit (**Figure 2d**). Within the uppermost part (70–0 cm depth) the sediment is characterized by slope wash and colluvial deposits composed of soils and angular rock pieces (**Figure 2C**).

Samples for OSL dating were collected from both CQ subsections. The vertical sections were first cleaned and polished to ensure access to freshly exposed sediments. Stainless steel tubes (6 cm in diameter and 30 cm in length) were then inserted into the profile to obtain the samples. Once extracted from the profile, both the ends of the tube were immediately sealed by cotton and wrapped with dark-colored tape before being sealed in a black plastic bag in order to avoid light exposure and water loss. A total of five OSL samples were collected from section CQ (**Figure 2**). Additionally, radiocarbon dating samples were collected from the

middle-lower parts of the profile. They included eight aquatic plant leaves along with a terrestrial plant twig (**Figure 3**), as well as three BOM samples.

OSL DATING

Sample Preparation and Measurement

We selected quartz as the dating material due to the ease with which it can be bleached compared to feldspar. All OSL sample preparation and luminescence measurements were conducted under subdued red light in the Luminescence Dating Laboratory at the Qinghai Institute of Salt Lakes, Chinese Academy of Sciences. Then the outer 3 cm of sediment at the end of each steel tube were scraped away and reserved for measurements of water content and environmental dose rate. The unexposed middle section of the tube was used for equivalent dose (D_e) determination. The five raw samples were first treated with 10% HCl and 30% H_2O_2 to remove carbonates and organic materials, followed by wet sieving to obtain three fractions: grains smaller than 38 μm, middle-grained quartz (MG, 38–63 μm), and coarse-grained quartz (CG, 90–125 μm). All grains smaller than 38 μm were treated in glass cylinders using Stokes' law in order to

FIGURE 2 | Profile of section CQ. (A) section CQ1, (B) section CQ2, and (C) overall profile of section CQ. (a–d) are details of section CQ.

FIGURE 3 | Photos of radiocarbon dating samples. (a–d) Are aquatic plant remnants, (e) is terrestrial plant remnants.
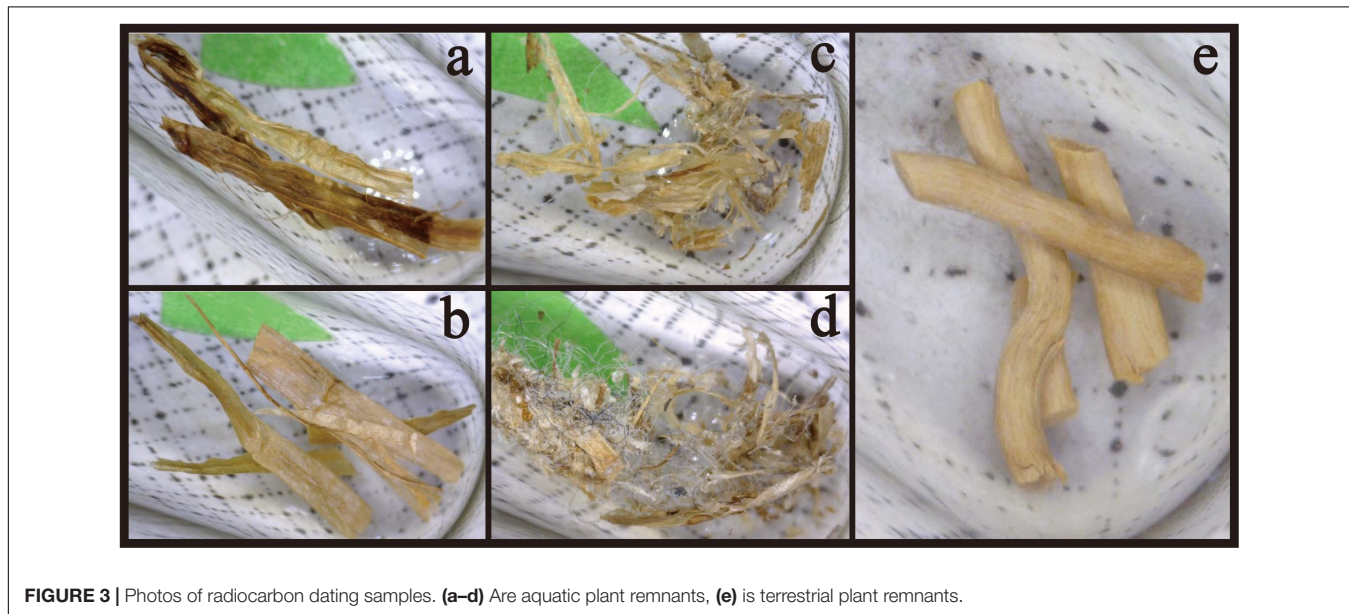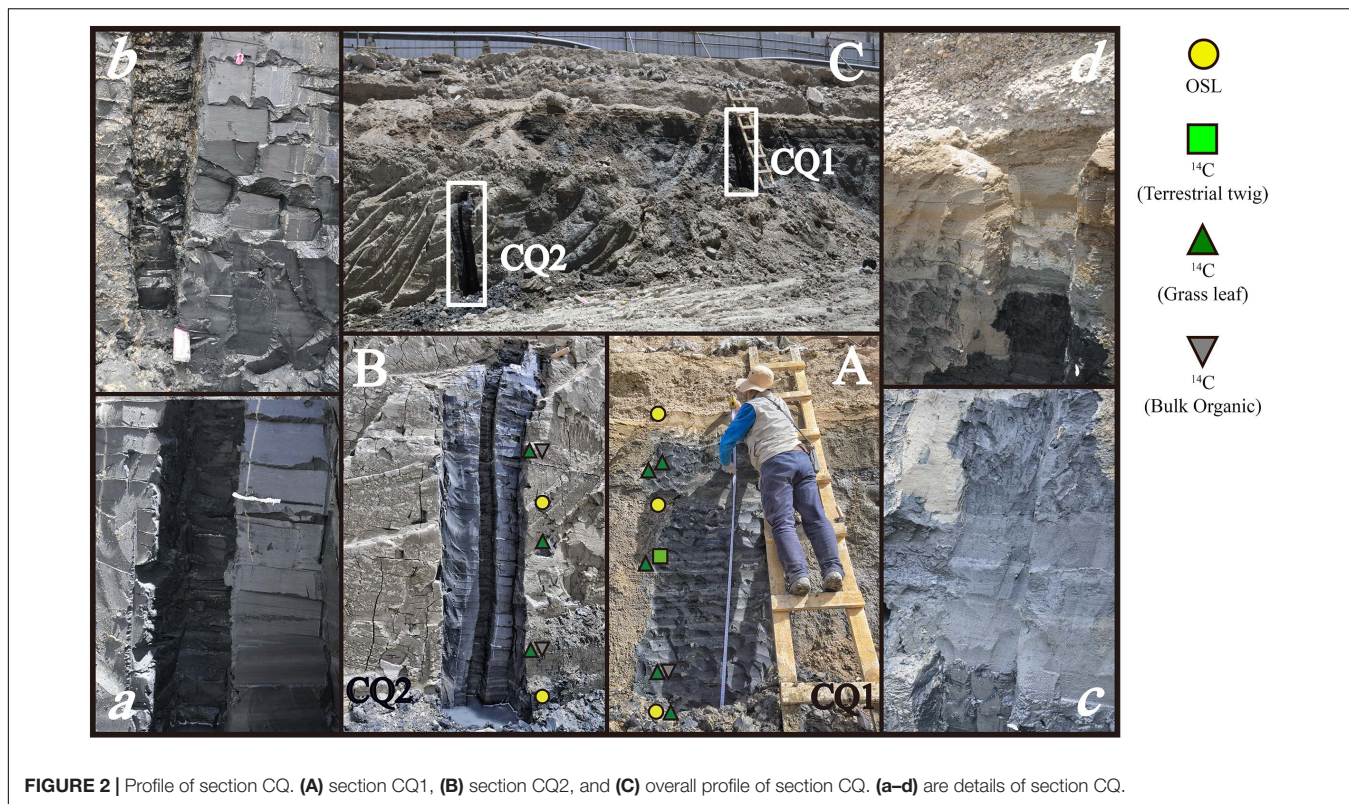
obtain fine-grained quartz (FG, 4–11 μm). The MG and FG were treated with silica saturated fluorosilicic acid (H_2SiF_6) for about 2 weeks, whereas the CG was etched with 40% HF for 60 min. All three fractions were then treated with 10% HCl to remove any fluorides, followed by the use of a magnet to remove any magnetic minerals. The purity of the isolated quartz was tested via infrared (IR) stimulation, with samples that showed obvious infrared stimulated luminescence (IRSL) signals retreated with H_2SiF_6 or

HF again until no obvious IRSL was observed in any sample. We also ensured that all feldspar was removed in order to protect against age underestimation (Duller, 2003; Roberts, 2007; Lai and Brückner, 2008). Finally, we chose sufficient fractions by the content of different grain sizes for D_e measurements (**Table 1**).

The quartz was mounted as a mono-layer on the central part (0.65 cm diameter) of a stainless-steel disc (0.97 cm diameter) using silicone oil. The OSL signal was measured using an

TABLE 1 | Luminescence dating results.

Sample ID	Depth (cm)	Grain size (μm)	K (%)	Th (μg/g)	U (μg/g)	Water content (%)	Dose rate (Gy/ka)	Number of aliquots	D_e (Gy)	Age (ka)	Age model
CQ1-A	145	90~125	2.83 ± 0.04	16.22 ± 0.7	2.722 ± 0.4	20 ± 5	3.91 ± 0.29	73	8.23 ± 0.27	2.1 ± 0.2	MAM-3
CQ1-B	221	90~125	2.86 ± 0.04	15.27 ± 0.7	2.21 ± 0.4	20 ± 5	3.74 ± 0.26	68	7.51 ± 0.52	2.0 ± 0.2	MAM-3
CQ1-91	375	38~63	2.90 ± 0.04	15.12 ± 0.7	2.82 ± 0.4	45 ± 5	2.76 ± 0.20	84	8.50 ± 0.50	3.1 ± 0.3	MAM-3
CQ2-26	445	38~63	2.93 ± 0.04	17.92 ± 0.7	3.19 ± 0.4	50 ± 5	2.65 ± 0.019	71	11.1 ± 1.04	4.2 ± 0.5	MAM-3
CQ2-60	552	4~11	2.55 ± 0.04	15.66 ± 0.7	6.14 ± 0.5	60 ± 5	2.35 ± 0.15	65	12.09 ± 0.41	5.1 ± 0.4	MAM-3

automated Risø TL/OSL-DA-20 reader. Laboratory irradiation was carried out using ^{90}Sr/^{90}Y sources mounted within the reader, with a dose rate of 0.086 Gy/s. The OSL signal was obtained after passage through a U-340 filter, while the IRSL signal was detected using a photomultiplier tube with the IRSL passing through BG-39 and coring-759 filters.

The environmental dose rate was calculated by measuring the radioactive element concentrations of surrounding sediments with a small contribution from cosmic rays. For all samples, U and Th concentrations and K contents were determined using inductively coupled plasma mass spectrometry (ICP-MS) analysis at the Institute of Earth Environment, Chinese Academy of Sciences in Xian. The cosmic ray dose was estimated for each sample as a function of depth, elevation, and geomagnetic latitude (Prescott and Hutton, 1994). The water content was calculated from sample weights measured before and after drying in an oven. The measured water contents of three deep lake samples CQ1-91, CQ2-26, and CQ2-60 were 43.8, 48.1, and 61.8%, respectively, and for the two shoreline samples CQ1-A and CQ1-B, the measured water contents were 20.5 and 19.7%, respectively. Due to water content variability during the burial period and based on the measured water content, approximations of measured water content were used to calculate OSL ages; an error of 5% of the measured water content was applied given the uncertainty of water changes in the lake sediments after burial (**Table 1**). The α-value for fine-grained quartz and middle-grained quartz was taken as 0.035 ± 0.003 (Lai et al., 2008). Radionuclide concentrations, water content, and dose rates are summarized in **Table 1**. Lastly, we converted the elemental concentrations into annual dose rates according to Aitken (1998).

Luminescence Characteristics

The equivalent dose for each sample was measured using the single aliquot regenerative dose (SAR) protocol (Murray and Wintle, 2000). For each sample, at least 65 aliquots were measured by SAR. The OSL signal was calculated using the integral of the initial 0.64 s of the OSL signals minus the last 8 s. The characteristics of the quartz luminescence growth and decay curves for sample CQ1-A and CQ2–60 are shown in **Supplementary Figure 1**. It is important to investigate the influence of preheating on the charge transfer from light-insensitive traps to light-sensitive ones, a process called thermal transfer (Aitken, 1998). To select the appropriate preheat conditions for D_e determination using the SAR protocol, a preheat temperature plateau test was conducted for samples CQ1-A and CQ1-B. Preheat temperatures from 140 to 240°C at

20°C intervals for 10 s were tested and the cut-heat was 140°C for 10 s, using a heating rate of 5°C/s. As a plateau was observed from 160 to 200°C, we therefore selected a preheat temperature of 200°C for routine D_e determination (**Supplementary Figure 2**). The suitability of the SAR procedure for D_e determination was further checked with a "dose recovery test" (Murray and Wintle, 2003). The dose recovery test was performed on sample CQ1-A. Six natural aliquots were stimulated for *c.* 56 h under direct sunlight. The aliquots were then given a laboratory dose of 9.2 Gy, close to the natural D_e (9.19 Gy). The measured D_e was 9.4 ± 1.8 Gy. Thus, the ratio of the measured to the given D_e was *c.* 1.02, suggesting that the SAR conditions were appropriate for D_e determination.

For OSL age calculation, because the sediments in nearby lakes within the TP did not experience long-distance transport or multiple sedimentation-transportation cycles, samples drawn from these lakes may be partially bleached, and the stimulated signal intensities will be low when compared with sediments from other regions, such as the Chinese Loess Plateau (Lee et al., 2009). To reduce this impact, CQ1–90 removed one test aliquot with abnormal data, CQ2–60 and CQ2–26 removed two test aliquots with abnormal data. Because each sample had at least 65 aliquots, the influence of removed data on the results could be ignored. The abnormal data did not occur in CQ1-A and CQ1-B. **Supplementary Table 1** shows the raw data for D_es. Moreover, Arnold et al. (2007) proposed the single-aliquot age selection model to determine whether the 3-parameter minimum-age model (MAM-3) or the central-age model (CAM) was applied to calculate the D_es. We used the R-language-based luminescence data analysis package "numOSL" to select the suitable age model (Peng et al., 2013), with all the samples' D_es ultimately determined using MAM-3 (**Table 1**).

RADIOCARBON DATING

Radiocarbon dating of 12 samples took place at Beta Analytic Inc. (Miami, FL, United States). Eight samples were APR, three samples were BOM, and the final sample was a terrestrial plant twig. Three samples (BOM) were simply treated with acid washes to remove any carbonates, whereas the nine plant samples were pre-treated with acid/alkali/acid to remove carbonates and mobile humic acids. They were then subjected to accelerator mass spectrometry (AMS) to measure their ^{14}C ratios. The calibration of ^{14}C dates was performed using the "CALIB 8.1.0" program (Stuiver et al., 2021) and the IntCal20 calibration curve (Reimer et al., 2020). The ^{13}C/^{12}C ratios (δ^{13}C, ‰) of

all dating materials were measured using an isotope ratio mass spectrometer (IRMS). All ^{14}C ages from section CQ are summarized in **Table 2**. Radiocarbon ages and OSL ages are shown together against the depth scale in **Figure 4**.

RESULTS AND DISCUSSION

OSL Ages

Our results showed that the ages for all five OSL samples increased with respect to their depth within the section, indicating that these lacustrine sediments were deposited between 5 and 2 ka BP (**Table 2**). The uppermost sample CQ1-A, just below the paleo-shoreline deposits, returned an OSL age of 2.1 ± 0.2 ka BP. Accordingly, the oldest OSL age was 5.1 ± 0.4 ka BP, which was from the sample collected from the bottom of section CQ (**Figure 2** and **Table 2**). The ages of the three mid-depth samples collected from 220, 375, and 445 cm were 2.0 ± 0.2 ka BP, 3.1 ± 0.3 ka BP, and 4.2 ± 0.5 ka BP, respectively (**Table 2**). We suggest that the lake level was higher than section CQ (4,664 m) during the interval from 5.1 to 3.1 ka BP on account of the lacustrine nature of the sediments, and because the paleo-shoreline deposits within the upper part of the section were deposited at *c.* 2 ka BP—the lake has further regressed since then. Our speculation is consistent with previous research indicating that the lake level of Zhari Namco declined by 42.5 m between 3.9 and 2.0 ka BP (from 4,680.6 to 4,637.9 m) (Chen et al., 2013).

Equivalent Dose and Dose Rate of OSL Ages

During the deposition process, the OSL signal bleaching degree is the key factor affecting the accuracy of D_e determination in lacustrine sediments. In different minerals, quartz is more easily bleached than feldspar (Long et al., 2010). According to the OSL dating results from other lacustrine sediments within the TP (Long et al., 2012), the OSL signal of lacustrine sediments was well bleached during the deposition. In our study, the OSL signal quickly decreased to background levels

within the first 2 s (**Supplementary Figure 1**), indicating that it was dominated by the fast component (Singarayer and Bailey, 2003). It also suggested that the quartz in our samples was relatively bright, which should have bleached easily when the grains were exposed to sunlight. Even so, our samples showed broad D_e distributions that may have been heterogeneously bleached before deposition (**Supplementary Figure 3**). To mitigate the influence of partial bleaching on age estimation, we used MAM-3 to calculate D_es. Moreover, in D_e determination using the SAR protocol, inaccuracies may have been caused by improper heating conditions. However, dose recovery tests and preheat temperature plateau tests showed that D_es was measured correctly for all samples from the CQ section using the SAR protocol (Aitken, 1998; Murray and Wintle, 2003). Therefore, we concluded that the OSL dating correctly measured and calculated D_e in this study.

The dose rate is determined by the content of the radionuclides in the sediments. It is usually assumed the dose rate of a sample is constant during the burial period in OSL dating (Zhang et al., 2007). Cupper (2006) measured sediment radioactivity from three salt lakes within southeastern Australia, finding it was in secular equilibrium from one of the salt lakes. Sediment radioactivity was in disequilibrium in the other two salt lakes, but this had a minimal effect on the dose rate. As shown in **Table 1**, the radionuclides contents of our samples were roughly constant, similar to other lacustrine sediments within the TP (Long et al., 2014; Hu et al., 2017). This suggests that radionuclides disequilibrium was likely to be absent in our samples (Long et al., 2015).

Water content is also the main factor affecting dose rate except for radionuclides. The water molecules in the sediments will absorb some radiation energy from the environment, reducing the absorption of the radiation energy by the sediments themselves (Zhang et al., 2007). In the field, we found that sediments in the profile were well preserved in a permanently frozen condition (the elevation of the site was *c.* 4,664 m), the water content was stable throughout their burial stage, and

TABLE 2 | Radiocarbon dating results.

Lab code	Sample code	Depth (cm)	Materials	$\delta^{13}C$ (‰)	Pmc	Conventional ^{14}C age (a BP)	Calibrated 2σ age range* (Cal a BP)
Beta-498519	CQ1-24	178	Grass leaf	−8.7	58.19 ± 0.22	4,350 ± 30	4,849–5,027
Beta-498520	CQ1-27	184	Grass leaf	−10.7	56.90 ± 0.21	4,530 ± 30	5,052–5,313
Beta-498521	CQ1-61	258	Terrestrial twig	−23	61.62 ± 0.23	3,890 ± 30	4,189–4,417
Beta-498522	CQ1-88B	339	Bulk organic	−23.1	46.04 ± 0.17	6,230 ± 30	7,011–7,253
Beta-498523	CQ2-16G	400	Grass leaf	−11.5	57.11 ± 0.21	4,500 ± 30	5,046–5,301
Beta-498524	CQ2-16B	400	Bulk organic	−22.4	43.92 ± 0.16	6,610 ± 30	7,431–7,569
Beta-498528	CQ2-2B	525	Bulk organic	−21.8	45.19 ± 0.17	6,380 ± 30	7,177–7,421
Beta-499906	CQ1-88G	339	Grass leaf	−4.3	56.97 ± 0.21	4,520 ± 30	5,051–5,309
Beta-501268	CQ1-64	267	Grass leaf	−9	56.05 ± 0.21	4,650 ± 30	5,315–5,466
Beta-501269	CQ1-100	375	Grass leaf	−7.3	55.64 ± 0.21	4,710 ± 30	5,324–5,575
Beta-501270	CQ2-1	475	Grass leaf	−15.5	55.08 ± 0.21	4,790 ± 30	5,475–5,588
Beta-501271	CQ2-2G	525	Grass leaf	−9.5	52.61 ± 0.20	5,160 ± 30	5,766–5,994

The ^{14}C ages were calibrated to calendar years using the CALIB 8.1.0 program (Stuiver et al., 2021) with the internationally agreed IntCal20 data set (Reimer et al., 2020).

FIGURE 4 | Stratigraphy of the lacustrine sediment sequences and the ages of section CQ discussed in the text. The three shaded areas are the age-depth models of lacustrine sediment. The yellow shaded area is the OSL age-depth model, and the green and gray shaded areas are the age-depths of aquatic plant remnants and bulk organic matter, respectively. Three dotted lines are the median ages. Because there was only one ^{14}C age of TPR, we did not use it to build the age-depth model.

no evidence of a disturbance was observed from the structural features of the profile. Therefore, the measured water content at present could represent the real water content of sediments from section CQ during the burial period.

^{14}C Ages

The twig, with a depth of 258 cm (CQ1–61), had a ^{14}C age of 4,189–4,417 Cal a BP. The aquatic plant leaf, although coming from a similar depth of 267 cm (CQ1–64), returned a ^{14}C age of 5,315–5,466 Cal a BP. Moreover, at depths of 339, 400, and 525 cm, the ^{14}C ages of these aquatic plant leaf samples were 5,051–5,309, 5,046–5,301, and 5,766–5,994 Cal a BP, respectively. However, at a similar depth, the ^{14}C ages of BOM were 7,011–7,253, 7,431–7,569, and 7,177–7,421 Cal a BP. The rest of aquatic plant leaves were sampled at depths of 178, 184, 375, and 475 cm, with reported ^{14}C ages of 4,849–5,027, 5,052–5,313, 5,324–5,575, and 5,475-5,588 Cal a BP, respectively.

^{14}C Ages of Terrestrial Plant Remnants

In general, the ^{14}C ages of TPR are not affected by LRE, and their ages are often considered to be consistent with those of the sedimentary horizons in which they are found (Hou et al., 2012). However, the ^{14}C age of the terrestrial twig (CQ1–61, 4,372 a) was roughly 2.3 ka older than the OSL sample (CQ1-B, 2.0 ± 0.2 ka BP) taken at a similar stratigraphic depth in section CQ. It is worth noting, however, that this discrepancy could possibly be explained due to a delay between the death of the twig and its ultimate transportation to, and burial within, the lacustrine sediments of the lake (Chen et al., 2017).

^{14}C Ages of Aquatic Plant Remnants

As shown in **Table 2** and **Figure 4**, the ^{14}C ages of APR were older than the OSL ages at similar depths, an inconsistency that was possibly due to the influence of LRE. This line of reasoning is supported, firstly, by the massive marine carbonate rocks which are widely distributed throughout the Coqen Basin (Zhong et al., 2010). These rocks have been eroded by precipitation runoff recharge and glacial meltwater from the catchment area, which enters the lake as dissolved inorganic carbon (DIC). In addition to DIC, dissolved organic carbon (DOC) and particulate organic carbon (POC) enters the lake by various means (Chen H. et al., 2019; Meng et al., 2020), with some underground

brine water also infiltrating the lake via underlying faults (Fontes et al., 1996). Secondly, Zhari Namco is centrally located within the TP, which is one of the coldest and most arid regions. Extensive evaporation has resulted in a high concentration of carbon ions in the water, with the lake struggling to maintain equilibrium with atmospheric carbon (Zhou et al., 2020). Aquatic plants are therefore absorbing greater quantities of old or dead carbon (Olsson, 2009; Meng et al., 2020), possibly leading to inflated age estimates.

^{14}C Ages of Bulk Organic Matter

The ^{14}C ages for BOM were consistently older than that of OSL and ^{14}C ages for APR of similar depth (**Figure 4**). However, determining the precise LRE to explain this discrepancy was complicated by the complex nature of BOM. Firstly, in addition to the carbon disequilibrium between water and atmosphere, as well as the abundance of old and dead carbon from the catchment area, microalgae and bacteria which lived in Zhari Namco represent yet another source of LRE affecting BOM (Meyers and Ishiwatari, 1993; Li et al., 2015; Chen H. et al., 2019). Secondly, bulk masses of terrestrial organic matter and external POC can be directly deposited without dissolution in lacustrine sediments, which can also produce inflated ^{14}C age estimates for BOM (Meng et al., 2020). Moreover, HCL washing, which is typically used to remove carbonate during the preparation of BOM samples, sometimes has the unintended corollary of

mixing carbonate remnants into the organic material, which can also make the age of the sample appear older than it actually is (Harkness, 1975; Gilet-Blein et al., 1980). However, because all ^{14}C samples were pretreated and dated in Beta's laboratory, we did not know the exact details for this performance, hence this factor could not easily be estimated in this study. In conclusion, the ^{14}C ages of BOM from Zhari Namco were also clearly subject to a host of LRE, and caution should be taken before drawing inferences from ^{14}C ages based on this material.

Implications for Lacustrine Sediments Dating in Zhari Namco

Although the error margins for radiocarbon dating are lower compared with luminescence dating, and TPR are generally exempt from the influence of LRE (Hou et al., 2012), TPR are nonetheless rare in the lacustrine sediments of the TP due to low vegetation cover. Additionally, as terrestrial plants typically grow on the land surrounding the lake, they are not necessarily deposited directly into the lake upon death. This means that the timing of both their death and their retention on land remains uncertain (Chen et al., 2017), further illustrating the caution required when using the ^{14}C ages of TPR. Most ^{14}C ages from loess sediments (Wang et al., 2014; Song et al., 2015; Song et al., 2017; Cheng et al., 2019) have underestimated ages. In contrast, due to the effects of LRE, the ^{14}C ages of APR and BOM are overestimated in Zhari Namco. This phenomenon has also been
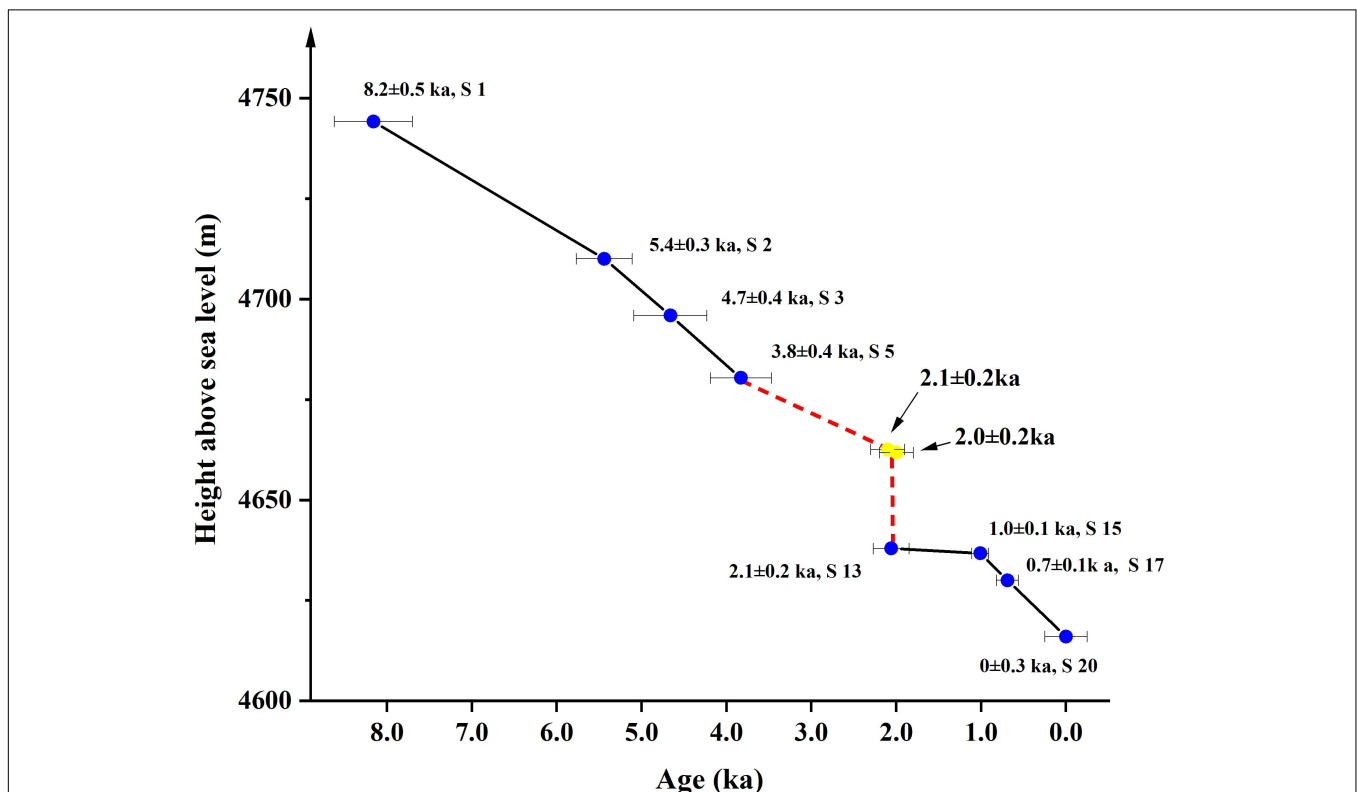
FIGURE 5 | OSL ages plotted against elevation for the 10 paleo-shorelines sediments of Zhari Namco. Blue circles are the ages of each shoreline from Chen et al. (2013). Yellow circles are the OSL ages of the CQ section.

observed in QingHai Lake (Meng et al., 2020), Tangra Yumco (Long et al., 2014), and Linggo Co (Hu et al., 2017), all of which contain BOM with ^{14}C ages older than that of stratigraphically associated aquatic plant material, and all ^{14}C ages of APR and BOM appearing older than its actual age.

OSL dating is not affected by the LRE of lacustrine sediments. The equivalent dose and dose rate used in the calculation of OSL age in this study were reliable. The OSL ages were in stratigraphic sequence order, with no age reversals, and we used MAM-3 to mitigate the influence of partial bleaching on age estimation and to make sure that any overestimation of the equivalent dose had less impact on OSL ages (Peng et al., 2013; Shi et al., 2017). An age-depth model for the CQ section's lacustrine sediments was established using the Bacon age-depth modeling package in "R" software (Blaauw and Christen, 2011) for five OSL ages, eight ^{14}C ages of APR, and three ^{14}C ages of BOM. As shown in **Figure 4**, age-depth model for OSL calculations found that for the ^{14}C ages of APR and ^{14}C ages of BOM, the average sedimentation rates of section CQ section *c.* 1.06 mm·a^{-1}, *c.* 5.03 mm·a^{-1}, *c.* 19.8 mm·a^{-1}. The average sedimentation rate was *c.* 1.03 mm·a^{-1} within Linggo Co (Hu et al., 2017), which was also similar to the average sedimentation rate found by using OSL age from section CQ. Due to this convergence in multiple lines of evidence, we are confident of the general reliability of OSL ages in section CQ.

The chronology framework for a series of paleo-shorelines and section CQ in Zhari Namco showed that lake level dropped by 128 m since *c.* 8.2 ka BP (Chen et al., 2013) (**Figure 5**). Notably, there was a "dog-leg" change in **Figure 5**. Based on the OSL ages and the sedimentary facies of section CQ, the sediments from the bottom experienced continuous sedimentation within a deep and stable lake environment. As depth decreased, sediments changed to a high-energy shoreline deposition (**Figure 4**). This meant that the lake level of Zhari Namco dropped rapidly between *c.* 5.1 ka BP and *c.* 2.0 ka BP, which was also consistent with a similarly rapid decline in the levels of Seling Co Lake and Zabuye Lake—reported as occurring during the late Holocene (Shi et al., 2017; Jonell et al., 2020). Therefore, we suggested that the rapidly dropping lake level caused the "dog-leg" change. Another possible cause might be that section CQ was located at the mountainous area far from the lakefront area, with undulating landforms and significant elevation change.

The major reason behind the dropping lake level may have been the weakening Indian summer monsoon, which caused the climate in Zhari Namco to change from relatively warm-humid to cold-arid during this period (Chen et al., 2013). Because of this, the recharge of the catchment area into the lake also underwent a gradual decrease during this period. Moreover, it was clear that the RAs were not constant, neither in APR nor in BOM (**Figure 6**). This was probably related to the drop in lake level. From stratigraphy and age fluctuation, during *c.* 5.1 ka BP to *c.* 2 ka BP, Zhari Namco experienced a drop in lake level. With this decrease, the RAs of APR increased from *c.* 0.1 ka to *c.* 4.1 ka
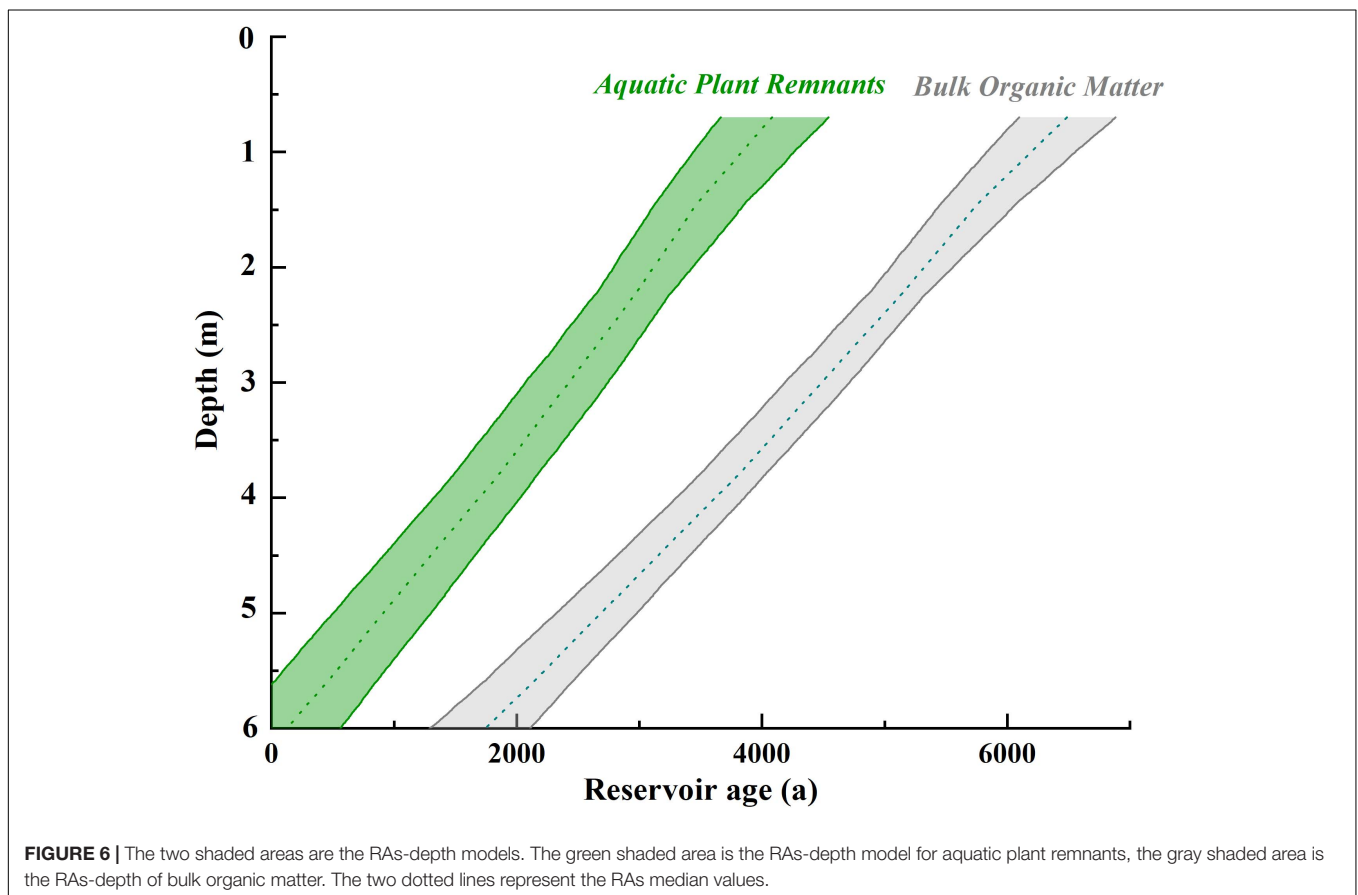
FIGURE 6 | The two shaded areas are the RAs-depth models. The green shaded area is the RAs-depth model for aquatic plant remnants, the gray shaded area is the RAs-depth of bulk organic matter. The two dotted lines represent the RAs median values.

(6–0.7 m core depth), and the RAs of BOM increased from *c.* 1.7 ka to *c.* 6.5 ka (6–0.7 m core depth). We suggest that the major contributor to LRE variation in Zhari Namco is salinity. Salinity, in addition to being associated with climate-driven fluctuations in lake capacity and level (Fontes et al., 1996; Wu et al., 2007), has been tightly influenced by changes in carbon ion concentration (Xu et al., 2006; Lei et al., 2010; Li and Liu, 2012, 2014; Li et al., 2015; Batanero et al., 2017; Zhou et al., 2020), causing RAs to increase or decrease in different periods. During warm-humid periods and the attendant increase in lake capacity and water level, lake desalination would occur, which, accompanied by a decrease in carbon ion concentration (Yu et al., 2016), caused a concomitant decrease in RAs. However, the opposite situation occurred during cold-arid periods, which caused RAs to increase. Similar results were found in Qinghai Lake: Chongyi et al. (2018) suggested that the highest RAs may have occurred when the lake had its highest salinity and lowest water levels. In addition, the RAs of BOM were greater than APR, possibly due to the increased complexity of the LRE sources acting on it (Gilet-Blein et al., 1980). Either way, because of the noted influence of LRE, the ^{14}C age estimates of APR and BOM cannot be considered to be wholly accurate.

CONCLUSION

In this study, radiocarbon and OSL dating were used to date lacustrine sediments from Zhari Namco Lake in the southern Tibetan Plateau. Through the comparison and analysis of ^{14}C and OSL ages, we found that the OSL dating can produce reliable ages and has good potential for lacustrine sediments dating. By contrast, even though ^{14}C dating is a mature dating method with high accuracy for dating lacustrine sediments, ^{14}C ages of both aquatic plants remnants and BOM are negatively impacted by LRE, which can lead to apparent ^{14}C ages being older than their actual ages. During warm-humid periods/cold-arid periods, RAs decrease/increase in response to higher/lower water levels, indicating that fluctuating that RA values are clearly associated with variations in the overarching hydrological regime. Due to the multitude of factors affecting LRE, it can be difficult to obtain reliable ages from APR and BOM, especially as the timing of both the death and ultimate deposition of terrestrial plants is often impossible to establish. In summary, OSL ages were more reliable than ^{14}C ages in this study. Accordingly, we suggest that radiocarbon dating alone may be inappropriate for dating lacustrine sediments and that OSL dating could be applied when evaluating the reliability of ^{14}C ages. Only by exploring areas of agreement and disagreement between multiple dating methods can we work toward building an accurate chronological framework for lacustrine sediments within the TP.

DATA AVAILABILITY STATEMENT

The original contributions presented in the study are included in the article/**Supplementary Material**, further inquiries can be directed to the corresponding author/s.

AUTHOR CONTRIBUTIONS

LC designed the research. LC, YW, XZ, TC, DG, and FA performed the research. LC and YW analyzed the data and wrote the manuscript. All authors contributed to the article and approved the submitted version.

FUNDING

ACKNOWLEDGMENTS

We thank two reviewers for their valuable suggestions and comments on the manuscript. Furthermore, we thank X.-J. Liu who firstly designed and guided the performance of this study; Aijun Sun and Jun Zhou for their help in the field; and Guoqiang Li, Jun Peng, and He Yang for help with analysis of the data.

SUPPLEMENTARY MATERIAL

The Supplementary Material for this article can be found online at: https://www.frontiersin.org/articles/10.3389/feart.2021.640172/full#supplementary-material

Supplementary Figure 1 | Characteristics of quartz luminescence growth curves and decay curves of samples CQ1-A and CQ2–60.

Supplementary Figure 2 | Preheat plateau test results for 90–125 μm quartz in samples CQ1-A and CQ1-B.

Supplementary Figure 3 | Radial plots showing distributions of equivalent dose (D_e) and uncertainties of the OSL samples.

Supplementary Table 1 | The raw data for equivalent dose (D_e) determination; the red numbers indicate abnormal data, which were removed before further analysis.

REFERENCES

Aitken, M. J. (1998). *An Introduction to Optical Dating.* Oxford: Oxford University Press.

An, F. Y., Liu, X. J., Zhang, Q. X., Wang, Y. X., Chen, T. Y., Yu, L. P., et al. (2018). Drainage geomorphic evolution in response to paleoclimatic changes since 12.8 ka in the eastern Kunlun Mountains, NE Qinghai-Tibetan Plateau. *Geomorphology* 319, 117–132. doi: 10.1016/j.geomorph.2018.07.016

Arnold, L. J., Bailey, R. M., and Tucker, G. E. (2007). Statistical treatment of fluvial dose distributions from southern Colorado arroyo deposits. *Quat. Geochronol.* 2, 162–167. doi: 10.1016/j.quageo.2006.05.003

Ascough, P., Cook, G. T., Kinch, H., Dunbar, E., Church, M. J., Einarsson, A., et al. (2011). An Icelandic fresh-water radiocarbon reservoir effect: implications for lacustrine 14C chronologies. *Holocene* 21, 1073–1080. doi: 10.1177/0959683611400466

Batanero, G. L., León-Palmero, E., Li, L. L., Green, A. G., Rendón-Martos, M., Suttle, C. A., et al. (2017). Flamingos and drought as drivers of nutrients and microbial dynamics in a saline lake. *Sci. Rep.* 7:12173. doi: 10.1038/s41598-017-12462-9

Blaauw, M., and Christen, J. (2011). Flexible paleoclimate age-depth models using an autoregressive gamma process. *Bayesian Anal.* 6, 457–474. doi: 10.1214/ba/1339616472

Chen, F. H., Huang, X. Z., Zhang, J. W., Holmes, J. A., and Chen, J. H. (2006). Humid Little Ice age in arid central Asia documented by Bosten Lake, Xinjiang, China. *Sci. China Ser. D Earth Sci.* 49, 1280–1290.

Chen, H., Zhu, L. P., Ju, J. T., Wang, J. B., and Ma, Q. F. (2019). Temporal variability of 14C reservoir effects and sedimentological chronology analysis in lake sediments from Chibuzhang Co, North Tibet (China). *Quat. Geochronol.* 52, 88–102. doi: 10.1016/j.quageo.2019.02.009

Chen, T. Y., Lai, Z. P., Liu, S. W., Wang, Y. X., Wang, Z. T., Miao, X. D., et al. (2019). Luminescence chronology and palaeoenvironmental significance of limnic relics from the Badain Jaran Desert, northern China. *J. Asian Earth Sci.* 177, 240–249. doi: 10.1016/j.jseaes.2019.03.024

Chen, T. Y., Liu, S. W., Lai, Z. P., Wang, Z. T., Han, F. Q., and Wang, Y. X. (2017). A preliminary study of AMS 14C dating of young lacustrine sediments in the Badain Jaran Desert. *J. Salt Lake Res.* 25, 60–66.

Chen, Y. W., Zhong, Y. Q., Li, B., Li, S. H., and Aitchison, J. C. (2013). Shrinking lakes in Tibet linked to the weakening Asian monsoon in the past 8.2ka. *Quat. Res.* 80, 189–198. doi: 10.1016/j.yqres.2013.06.008

Cheng, P., Burr, G., Zhou, W. J., Chen, N., Hou, Y. Y., Du, H., et al. (2019). The deficiency of organic matter 14C dating in Chinese Loess-paleosol sample. *Quat. Geochronol.* 56:101051. doi: 10.1016/j.quageo.2019.101051

Chongyi, E., Sun, Y. J., Liu, X. J., Hou, G. L., Lv, S. C., Yuan, J., et al. (2018). A comparative study of radiocarbon dating on terrestrial organisms and fish from Qinghai Lake in the northeastern Tibetan Plateau, China. *Holocene* 28, 1712–1719. doi: 10.1177/0959683618788671

Cupper, M. L. (2006). Luminescence and radiocarbon chronologies of playa sedimentation in the Murray Basin, Southeastern Australia. *Quat. Sci. Rev.* 25, 2594–2607. doi: 10.1016/j.quascirev.2005.09.011

Duller, G. A. T. (2003). Distinguishing quartz and feldspar in single grain luminescence measurements. *Radiat. Meas.* 37, 161–165. doi: 10.1016/S1350-4487(02)00170-1

Fontes, J. C., Gasse, F., and Gibert, E. (1996). Holocene environmental changes in Lake Bangong basin (Western Tibet). Part 1: chronology and stable isotopes of carbonates of a Holocene lacustrine core. *Palaeogeogr. Palaeoclimatol. Palaeoecol.* 120, 25–47. doi: 10.1016/0031-0182(95)00032-1

Gilet-Blein, N., Marien, G., and Evin, J. (1980). Unreliability of 14C dates from organicmatter of soils. *Radiocarbon* 22, 919–929. doi: 10.1017/S0033822200010328

Harkness, D. (1975). "The role of the archaeologist in C-14 measurement," in *Radiocarbon: Calibration and Prehistory*, ed. T. Watkins (Edinburgh: Edinburgh University Press), 128–135.

Hou, J. Z., D'Andrea, W. J., and Liu, Z. H. (2012). The influence of 14C reservoir age on interpretation of paleolimnological records from the Tibetan Plateau. *Quat. Sci. Rev.* 48, 67–79. doi: 10.1016/j.quascirev.2012.06.008

Hou, J. Z., Huang, Y. S., Brodsky, C., Alexandre, M. R., Mcnichol, A. P., King, J. W., et al. (2010). Radiocarbon dating of individual lignin phenols: a new approach for establishing chronology of late quaternary lake sediments. *Anal. Chem.* 82, 7119–7126. doi: 10.1021/ac100494m

Hu, G., Yi, C. L., Zhang, J. F., Cao, G. R., Pan, B. L., Liu, J. H., et al. (2017). Chronology of a lacustrine core from Lake Linggo Co using a combination of OSL, 14C and 210Pb dating: implications for the dating of lacustrine sediments from the Tibetan Plateau. *Boreas* 47, 656–670. doi: 10.1111/bor.12291

Jonell, T. N., Aitchison, J. C., Li, G. Q., Shulmeister, J., Zhou, R. J., and Zhang, H. X. (2020). Revisiting growth and decline of late Quaternary mega-lakes across the south-central Tibetan Plateau. *Quat. Sci. Rev.* 248:106475. doi: 10.1016/j.quascirev.2020.106475

Kang, S. G., Wang, X. L., Roberts, M. H., Duller, G. A. T., Song, Y. G., Liu, W. G., et al. (2020). Increasing effective moisture during the Holocene in the semiarid regions of the Yili Basin, Central Asia: evidence from loess sections. *Quat. Sci. Res.* 246:106553. doi: 10.1016/j.quascirev.2020.106553

Lai, Z. P., and Brückner, H. (2008). Effects of feldspar contamination on equivalent dose and the shape of growth curve for OSL of silt-sized quartz extracted from Chinese loess. *Geochronometria* 30, 49–53. doi: 10.2478/v10003-008-0010-0

Lai, Z. P., Zöllerr, L., Fuchs, M., and Brückner, H. (2008). Alpha efficiency determination for OSL of quartz extracted from Chinese loess. *Radiat. Meas.* 43, 767–770. doi: 10.1016/j.radmeas.2008.01.022

Lee, J., Li, S. H., and Aitchison, J. C. (2009). OSL dating of paleoshorelines at Lagkor Tso, western Tibet. *Quat. Geochronol.* 4, 335–343. doi: 10.1016/j.quageo.2009.02.003

Lei, Y. B., Zhang, H. C., Li, S. J., Yang, L. Q., Yao, S. C., Li, C. H., et al. (2010). Variation of 13C value in authigenic carbonates from Zigetang Co, Tibetan Plateau since 1950 AD. *J. Lake Sci.* 1, 143–150. doi: 10.18307/2010.0120

Li, C. G., Zheng, Y., Wang, M. D., Sun, Z., and Jin, C. S. (2021). Refined dating using palaeomagnetic secular variations on a lake sediment core from Guozha Co, northwestern Tibetan Plateau. *Quat. Geochronol.* 62:101146. doi: 10.1016/j.quageo.2020.101146

Li, G. Q., Zhang, H. X., Liu, X. J., Yang, H., Wang, X. Y., Zhang, X. J., et al. (2020). Paleoclimatic changes and modulation of East Asian summer monsoon by high-latitude forcing over the last 130,000 years as revealed by independently dated loess-paleosol sequences on the NE Tibetan Plateau. *Quat. Sci. Rev.* 237:106283. doi: 10.1016/j.quascirev.2020.106283

Li, X. Z., and Liu, W. G. (2012). The stable oxygen isotopic composition of ostracoda Limnocythere inopinata Bird and its possible response to water salinity in Lake Qinghai. *J. Lake Sci.* 24, 623–628. doi: 10.18307/2012.0417

Li, X. Z., and Liu, W. G. (2014). Water salinity and productivity recorded by ostracod assemblages and their carbon isotopes since the early Holocene at Lake Qinghai on the northeastern Qinghai-Tibet Plateau, China. *Palaeogeogr. Palaeoclimatol. Palaeoecol.* 407, 25–33. doi: 10.1016/j.palaeo.2014.04.017

Li, X. Z., Liu, W. G., Zhou, X., Xu, L. M., and Cheng, P. (2015). A 700-year macrophyte productivity record inferred from isotopes of macrophyte remains and bulk carbonates in Lake Koucha, northeast Qinghai–Tibetan Plateau, China. *Quat. Int.* 430, 32–40. doi: 10.1016/j.quaint.2015.11.053

Liu, W. M., Hu, K. H., Carling, P. A., Lai, Z. P., Cheng, T., and Xu, Y. L. (2018). The establishment and influence of Baimakou paleo-dam in an upstream reach of the Yangtze River, southeastern margin of the Tibetan Plateau. *Geomorphology* 321, 167–173. doi: 10.1016/j.geomorph.2018.08.028

Liu, X. J., and Lai, Z. P. (2013). Optical dating of sand wedges and ice-wedge casts from Qinghai Lake area on the northeastern Qinghai-Tibetan Plateau and its palaeoenvironmental implications. *Boreas* 42, 333–341. doi: 10.1111/j.1502-3885.2012.00288.x

Liu, X. J., Lai, Z. P., Fan, Q. S., Long, H., and Sun, Y. J. (2010). Timing for high lake levels of Qinghai Lake in the Qinghai-Tibetan Plateau since the Last Interglaciation based on quartz OSL dating. *Quat. Geochronol.* 5, 218–222. doi: 10.1016/j.quageo.2009.03.010

Liu, X. J., Lai, Z. P., Madsen, D., Yu, L. P., Liu, K., and Zhang, J. R. (2011). Lake level variations of Qinghai Lake in northeastern Qinghai-Tibetan Plateau since 3.7 ka based on OSL dating. *Quat. Int.* 236, 57–64. doi: 10.1016/j.quaint.2010.08.009

Liu, X. J., Lai, Z. P., Madsen, D., and Zeng, F. M. (2015). Last Deglacial and Holocene lake level variations of Lake Qinghai, northeastern Qinghai-Tibetan Plateau. *J. Quat. Sci.* 30, 245–257. doi: 10.1002/jqs.2777

Liu, X. J., Lai, Z. P., Yu, L. P., Sun, Y. J., and Madsen, D. B. (2012). Luminescence chronology of aeolian deposits from the Qinghai Lake area in the Northeastern Qinghai-Tibetan Plateau and its palaeoenvironmental implications. *Quat. Geochronol.* 10, 37–43. doi: 10.1016/j.quageo.2012.01.016

Liu, X. J., Xiao, G. Q., Chongyi, E., Li, X. Z., Lai, Z. P., Yu, L. P., et al. (2017). Accumulation and erosion of aeolian sediments in the northeastern Qinghai-Tibetan Plateau and implications for provenance to the Chinese Loess Plateau. *J. Asian Earth Sci.* 135, 166–174. doi: 10.1016/j.jseaes.2016.12.034

Liu, X. J., Zhang, X. J., Lin, Y. L., Jin, L. Y., and Chen, F. H. (2019). Strengthened Indian summer monsoon brought more rainfall to the western Tibetan Plateau during the early Holocene. *Sci. Bulletin.* 64, 1482–1485. doi: 10.1016/j.scib.2019.07.022

Liu, X. Q., Dong, H. L., Rech, J. A., Matsumoto, R., Yang, B., and Wang, Y. B. (2008). Evolution of Chaka Salt Lake in NW China in response to climatic change during the Latest Pleistocene–Holocene. *Quat. Sci. Rev.* 27, 867–879. doi: 10.1016/j.quascirev.2007.12.006

Long, H., Haberzettl, T., Tsukamoto, S., Shen, J., Kasper, T., Daut, G., et al. (2014). Luminescence dating of lacustrine sediments from Tangra Yumco (southern Tibetan Plateau) using post-IR IRSL signals from polymineral grains. *Boreas* 44, 139–152. doi: 10.1111/bor.12096

Long, H., Lai, Z. P., Frenzel, P., Fuchs, M., and Haberzettl, T.(2012). Holocene moist period recorded by the chronostratigraphy of a lake sedimentary sequence from Lake Tangra Yumco on the south Tibetan Plateau. *Quat. Geochronol.* 10, 136–142. doi: 10.1016/j.quageo.2011.11.005

Long, H., Lai, Z. P., Wang, N. A., and Li, Y. (2010). Holocene climate variations from Zhuyeze terminal lake records in East Asian monsoon margin in arid northern China. *Quat. Res.* 74, 46–56. doi: 10.1016/j.yqres.2010.03.009

Long, H., Lai, Z. P., Wang, N. A., and Zhang, J. R. (2011). A combined luminescence and radiocarbon dating study of Holocene lacustrine sediments from arid northern China. *Quat. Geochronol.* 6, 1–9. doi: 10.1016/j.quageo.2010.06.001

Long, H., Shen, J., Wang, Y., Gao, L., and Frechen, M. (2015). High-resolution OSL dating of a late Quaternary sequence from Lake Xingkai (NE Asia): chronological challenge of the "MIS 3a Mega-palaeolake"hypothesis in China. *Earth Planet. Sci. Lett.* 428, 281–292. doi: 10.1016/j.epsl.2015.07.003

Meng, B. W., Zhou, A. F., Zhang, Y. C., Song, M., Liu, W. G., Xie, Z. Q., et al. (2020). Downcore variations of carbon reservoir ages linked to lake level changes in northwest China. *Quat. Geochronol.* 60, 101–105. doi: 10.1016/j.quageo.2020.101105

Meyers, P. A., and Ishiwatari, R. (1993). Lacustrine organic geochemistry: anoverview of indicators of organic matter sources and diagensis in lakesediments. *Organ. Geochem.* 20, 867–900. doi: 10.1016/0146-6380(93)90100-P

Mischke, S., Aichner, B., Diekmann, B., Herzschuh, U., Plessen, B., Wünnemann, B., et al. (2010). Ostracods and stable isotopes of a late glacial and Holocene lake record from the NE Tibetan Plateau. *Chem. Geol.* 276, 95–103. doi: 10.1016/j.chemgeo.2010.06.003

Mischke, S., Weynell, M., Zhang, C., and Wiechert, U. (2013). Spatial variability of 14C reservoir effects in Tibetan Plateau lakes. *Quat. Int.* 313-314, 147–155. doi: 10.1016/j.quaint.2013.01.030

Morrill, C., Overpeck, J. T., Cole, J. E., Liu, K., Shen, C., and Tang, L. (2006). Holocene variations in the Asian monsoon inferred from the geochemistry of lake sediments in central Tibet. *Quat. Res.* 65, 232–243. doi: 10.1016/j.yqres.2005.02.014

Murray, A. S., and Wintle, A. G. (2000). Luminescence dating of quartz using and improved single-aliquot regenerative protocol. *Radiat. Meas.* 32, 571–577. doi: 10.1016/S1350-4487(99)00253-X

Murray, A. S., and Wintle, A. G. (2003). The single aliquot regenerative dose protocol: potential for improvements in reliability. *Radiat. Meas.* 37, 377–381. doi: 10.1016/S1350-4487(03)00053-2

Olsson, I. U. (2009). Radiocarbon dating history: early days, questions, and problems met. *Radiocarbon* 51, 1–43. doi: 10.2458/azu_js_rc.51.3477

Peng, J., Dong, Z. B., Han, F. Q., Long, H., and Liu, X. J. (2013). R package numOSL: numeric routines for optically stimulated luminescence dating. *Ancient TL* 31, 41–48.

Prescott, J. R., and Hutton, J. T. (1994). Cosmic ray contributions to dose rates for luminescence and ESR dating: large depths and long-term time variations. *Radiat. Meas.* 23, 497–500. doi: 10.1016/1350-4487(94)90086-8

Reimer, P. J., Austin, W. E. N., Bard, E., Bayliss, A., Blackwell, P. G., Ramsey, C. B., et al. (2020). The IntCal20 Northern hemisphere radiocarbon age calibration curve (0–55 cal kBP). *Radiocarbon* 62, 725–757. doi: 10.1017/RDC.2020.41

Roberts, H. M. (2007). Assessing the effectiveness of the double-SAR protocol in isolating a luminescence signal dominated by quartz. *Radiat. Meas.* 42, 1627–1636. doi: 10.1016/j.radmeas.2007.09.010

Shen, J., Liu, X. Q., Wang, S. M., and Matsumoto, R. (2005). Palaeoclimatic changes in the Qinghai lake area during the last 18,000 years. *Quat. Int* 136, 131–140. doi: 10.1016/j.quaint.2004.11.014

Shen, Z. X., Bloemendal, J., Mauz, B., Chiverrell, R. C., Dearing, J. A., Lang, A., et al. (2008). Holocene environmental reconstruction of sediment-source linkages at Crummock Water, English Lake District, based on magnetic measurements. *Holocene* 18, 129–140. doi: 10.1177/0959683607085604

Shi, X. H., Kirby, E., Furlong, K. P., Meng, K., Robinson, R., Lu, H. J., et al. (2017). Rapid and punctuated Late Holocene recession of Siling Co, central Tibet. *Quat. Sci. Rev.* 172, 15–31. doi: 10.1016/j.quascirev.2017.07.017

Singarayer, J. S., and Bailey, R. M. (2003). Further investigations of the quartz optically stimulated luminescence components using linear modulation. *Radiat. Meas.* 37, 451–458. doi: 10.1016/S1350-4487(03)00062-3

Song, Y. G., Lai, Z. P., Li, Y., Chen, T., and Wang, Y. X. (2015). Comparison between luminescence and radiocarbon dating of late Quaternary loess from the Ili Basin in Central Asia. *Quat. Geochronol.* 30, 405–410. doi: 10.1016/j.quageo.2015.01.012

Song, Y. G., Luo, D., Du, J. H., Kang, S. G., Cheng, P., Fu, C. F., et al. (2017). Radiometric dating of late Quaternary loess in the northern piedmont of South Tianshan Mountains: implications for reliable dating. *Geol. J.* 53:8. doi: 10.1002/gj.3129

Stuiver, M., and Braziunas, T. F. (1993). Modeling atmospheric 14C influences and 14C ages of marine samples to 10,000 BC. *Radiocarbon* 35, 137–189. doi: 10.1017/S0033822200013874

Stuiver, M., Reimer, P. J., and Reimer, R. W. (2021). *CALIB 8.1.0 [WWW program]*. Available online at: http://calib.org (accessed 01 January 2021).

Wang, H., Cui, P., Liu, D. Z., Liu, W. M., Bazai, N. A., Wang, J., et al. (2019). Evolution of a landslide-dammed lake on the southeastern Tibetan Plateau and its influence on river longitudinal profiles. *Geomorphology* 343, 15–32. doi: 10.1016/j.geomorph.2019.06.023

Wang, S. M., and Dou, H. S. (1998). *Chinese Lake Records*. Beijing: Science Press.

Wang, Y., Shen, J., Wu, J., Liu, X. Q., Zhang, E. L., and Liu, E. F. (2007). Hard-water effect correction of lacustrine sediment ages using the relationship between 14C levels in lake waters and in the atmosphere: the case of Lake Qinghai. *J. Lake Sci.* 19, 504–508. doi: 10.18307/2007.0502

Wang, Y. X., Chen, T. Y., Chongyi, E., An, F. Y., Lai, Z. P., Zhao, L., et al. (2018). Quartz OSL and K-feldspar post-IR IRSL dating of loess in the Huangshui river valley, northeastern Tibetan plateau. *Aeolian Res.* 33, 23–32. doi: 10.1016/j.aeolia.2018.04.002

Wang, Y. X., Chen, T. Y., Wu, C., Lai, Z. P., Guo, S. D., and Cong, L. (2019). Formation and evolution of the Xitaijinair Salt Lake in Qaidam Basin revealed by chronology. *Arid Land Geogr.* 42, 876–884. doi: 10.12118/j.issn.1000-6060.2019.04.19

Wang, Z. L., Zhao, H., Dong, G. H., Zhou, A. F., Liu, J. B., and Zhang, D. J. (2014). Reliability of radiocarbon dating on various fractions of loess-soil sequence for Dadiwan section in the western Chinese Loess Plateau. *Front. Earth Sci.* 8, 540–560. doi: 10.1007/s11707-014-0431-1

Wu, Y. H., Wang, S. M., Zhou, L. P., and Sun, Z. B. (2007). Modern reservoir age for 14C dating in DaiHai Lake. *Qua. Sci.* 4, 507–510. doi: 10.3321/j.issn:1001-7410.2007.04.005

Xu, H., Ai, L., Tan, L. C., and An, Z. S. (2006). Stable isotopes in bulk carbonates and organic matter in recent sediments of Lake Qinghai and their climatic implications. *Chem. Geol.* 235, 262–275. doi: 10.1016/j.chemgeo.2006.07.005

Yao, T. D., Thompson, L., Yang, W., Yu, W. S., Gao, Y., Guo, X. J., et al. (2012). Different glacier status with atmospheric circulations in Tibetan Plateau and surroundings. *Nat. Clim. Change* 2, 663–667. doi: 10.1038/nclimate1580

Yu, J. J., Zheng, M. P., Wu, Q., Wang, Y. S., Nie, Z., and Bu, L. Z. (2016). Natural evaporation and crystallization of Bangor salt lake water in Tibet. *Sci. Technol. Rev.* 34, 60–66. doi: 10.3981/j.issn.1000-7857.2016.05.006

Yu, S. Y., Shen, J., and Colman, S. M. (2007). Modeling the radiocarbon reservoir effect in lacustrine systems. *Radiocarbon* 49, 1241–1254. doi: 10.2458/azu_js_rc.49.3016

Zhang, J. F., Zhou, L. P., Yao, S. C., Xue, B., and Wang, X. L. (2007). Radiocarbon and optical dating of lacustrine sediments—a case study in Lake Gucheng. *Quat. Sci.* 4, 522–528. doi: 10.1016/S1872-5791(07)60044-X

Zhang, S., Zhang, J. F., Zhao, H., Liu, X. J., and Chen, F. H. (2020). Spatiotemporal complexity of the "Greatest lake Period" in the Tibetan Plateau. *Sci. Bull.* 65:16. doi: 10.1016/j.scib.2020.05.004

Zhong, Q., Fang, H., Liu, C. W., Li, X. C., Lu, J. Q., and Gao, B. T. (2010). The Paleozoic carbonate rocks depression of Coqen basin: evidence from geophysics on the Qinghai-Tibet Plateau, China. *Geol. Bull. China* 29, 870–879. doi: 10.3969/j.issn.1671-2552.2010.06.009

Zhou, A. F., Chen, F. H., Wang, Z. L., Yang, M. L., Qiang, M. R., and Zhang, J. W. (2011). Temporal change of radiocarbon reservoir effect in Sugan Lake, Northwest China during the Late-Holocene. *Radiocarbon* 51, 529–535. doi: 10.2458/azu_js_rc.51.3514

Zhou, K. E., Xu, H., Lan, J. H., Tan, D. N., Shen, E. G., Yu, K. K., et al. (2020). Variable Late Holocene 14C Reservoir Ages in Lake Bosten, Northwestern China. *Front. Earth Sci.* 7:601503. doi: 10.3389/feart.2020.601503

Zhu, D. G., Meng, X. G., Zhao, X. T., Shao, Z. G., Xu, Z. F., Yang, C. B., et al. (2004). Evolution of ancient large Lake in the Southeast of the Northern Tibetan Plateau. *Acta Geol. Sin.* 78, 982–992. doi: 10.1111/j.1755-6724.2004.tb00220.x

Zhu, L. P., Wu, Y. H., Wang, J. B., Lin, X., Ju, J. T., Xie, M. P., et al. (2008). Environmental changes since 8.4 ka reflected in the lacustrine core sediments from Nam Co, central Tibetan Plateau, China. *Holocene* 18, 831–839. doi: 10.1177/0959683608091801